



Contents lists available at ScienceDirect

Journal of King Saud University – Science

journal homepage: www.sciencedirect.com



Original article

Synthesis, physicochemical, optical, thermal and TD-DFT of (E)-N'-((9-ethyl-9H-carbazol-3-yl)-methylene)-4-methyl-benzene-sulfonohydrazide (ECMMBSH): Naked eye and colorimetric Cu²⁺ ion chemosensor

A.A. AlObaid^a, M. Suleiman^{b,*}, C. Jama^c, A. Zarrouk^d, I. Warad^{e,*}^a Department of Chemistry, College of Science, King Saud University, P.O. Box 2455, Riyadh 11451, Saudi Arabia^b Department of Chemistry, Science College, An-Najah National University, Nablus P.O. Box 7, Palestine^c Univ. Lille, CNRS, INRAE, Centrale Lille, UMR 8207, -UMET -Unité Matériaux et Transformations, F-59000 Lille, France^d Laboratory of Materials, Nanotechnology and Environment, Mohammed V University in Rabat, Faculty of Sciences, P.O. Box. 1014, Rabat, Morocco^e Department of Chemistry and Earth Sciences, PO Box 2713, Qatar University, Doha, Qatar

ARTICLE INFO

Article history:

Received 7 June 2021

Revised 15 September 2021

Accepted 27 September 2021

Available online 12 October 2021

Keywords:

Copper(II)

NMR

Schiff base

DFT

Sensation

ABSTRACT

Benzene-sulfonohydrazide (ECMMBSH) Schiff base has been made available in an excellent yield via reflux dehydrate of 4-methylbenzene-sulfonohydrazide with 9-ethyl-9H-carbazole-3-carbaldehyde in EtOH. The synthesis of the ECMMBSH was monitored via two main spectroscopic techniques FT-IR and UV-vis tools; ECMMBSH was characterized via MS, ¹H NMR, FT-IR, CHN-EA, TG/DTG, EDX, and UV-vis., analysis. Moreover, DFT-optimized, Molecular Electrostatic Potential (MEP) and MAC/NPA-charge models were performed for ECMMBSH. The HOMO/LUMO and Density of State (DOS) calculated energy levels were compared to Tuac experimental optical energy gap values in methanol. Additionally, the TD-DFT and UV-vis. experimental absorption behavior was matched under the same condition. Moreover, the chemo-sensation effect of the ECMMBSH towered Cu²⁺ ions via complexation was evaluated by naked eye in addition to the UV-vis spectrophotometric measurements.

© 2021 The Author(s). Published by Elsevier B.V. on behalf of King Saud University. This is an open access article under the CC BY-NC-ND license (<http://creativecommons.org/licenses/by-nc-nd/4.0/>).

1. Introduction

Schiff bases (S.B.) are an essential N-ligand class of organic material where the C=N— main functional group is capable to couple via treating the primary amine with ketones or aldehyde without catalysts or with utilizing pyridine or trimethylamine as basic catalysts or sulphuric, acetic, and hydrochloric acids as acidic catalysts (Shafaatian et al., 2016; Hossain et al., 1996; Abbasi et al., 2018; Pervaiz et al., 2019; Trzesowska-Kruszynska, 2012; Dehghani-Firouzabadi and Motevaseliyan, 2014; Johnson and Dhanaraj, 2020; Khan et al., 2012; Eckenhoff et al., 2012; Ahmadi

and Amani, 2012; Rajasekar et al., 2010; Konstantinovic et al., 2003; Routier et al., 1996; Wu et al., 2007). Aromatic Schiff base ligands are more common since it is more stable compared to the aliphatic analogue due to the aromatic conjugated structure that provides the azo-methine from free radical polymerization processes (Trzesowska-Kruszynska, 2012; Dehghani-Firouzabadi and Motevaseliyan, 2014; Johnson and Dhanaraj, 2020; Eckenhoff et al., 2012; Khan et al., 2012). The S.B ligands own many apps in several fields of chemistry, biology, and medicine. For example, several biological apps as antifungal, anti-inflammatory, anti-cancer, antibacterial, anti-plasmodial, antioxidant, anti-depressant and anti-corrosion have been reported (Sousa et al., 2012; Chatterjee et al., 2014; Badran et al., 2021; Badran et al., 2019; Warad et al., 2017c; Rouifi et al., 2019; Warad et al., 2014; Rbaa et al., 2019).

Moreover, S.B can be considered as one of the broadest and best chelates or polychelates N-ligands in the coordination of metal ions centers. Hydrazones Schiff base (HSB) containing azomethine functional group is a private type of such bases. HSB derivatives offering a better and broad diversity of medical activities like

* Corresponding authors.

E-mail addresses: suleimanshtaya@najah.edu (M. Suleiman), ismail.warad@qu.edu.qa (I. Warad).

Peer review under responsibility of King Saud University.



Production and hosting by Elsevier

<https://doi.org/10.1016/j.jksus.2021.101633>

1018-3647/© 2021 The Author(s). Published by Elsevier B.V. on behalf of King Saud University.

This is an open access article under the CC BY-NC-ND license (<http://creativecommons.org/licenses/by-nc-nd/4.0/>).

antiepileptic, antiviral, anti-inflammatory, antimicrobial, analgesic, antioxidant, anticholinesterase, and anticancer (Warad et al., 2017a; Saleemh et al., 2017; Warad et al., 2017b; Masoud et al., 2007; Despaigne et al., 2009; Al-Rimawi et al. 2016; Lindner et al., 2003).

Sulfonohydrazone Schiff bases have been made available mostly due to the chelate effect which made it an excellent ligand complex (Maurya et al., 2015). Their antifungal and antimicrobial biological properties received considerable attention (Hu et al., 2015), especially the ones with transition metal ions complexes containing heterocyclic parts (Jang et al., 2017). Binding of these ligands to the metal centers ions are desired due to the increased antifungal and antibacterial properties compared to the free ligands. Due to the colorimetric binding ability of such ligands to transition ions metal, there is still a need to develop a way of sensation to detect some of the heavy toxic elements like Cu^{2+} and Ru^{2+} in our environment via polychelate ligand (Das et al., 2019; Lu et al., 2003; Al-Zaqri et al., 2020a, 2020b; Warad et al., 2020).

Herein a new benzene-sulfonohydrazide Schiff base (ECMMBSH) was prepared then characterized via MS, ^1H NMR, CHN-EA, UV-vis., IR, and TG/DTG thermal analysis. Moreover, the ECMMBSH was computed using the DFT/level theory where the computed parameters were compared to the experimental results. Finally, the ECMMBSH naked eye colorimetric chemo-sensation of Cu^{2+} element was supported via UV-vis spectroscopy.

2. Experimental

2.1. Instrumentation and chemicals

CHN-EA was performed on an Elementar-Vario EL analyzer. TG/DTG was recorded on TGA Perkin-Elmer. FT-IR spectroscopy was carried out using 1000 FT-IR spectrometer Perkin-Elmer Spectrum. UV-Vis was recorded on a TU-1901 double-beam UV-visible spectrophotometer. All the chemicals were purchased from Sigma Company.

2.2. Synthesis of ECMMBSH

(0.032 mol) 4-methylbenzenesulfonohydrazide with (0.034 mol) 9-ethyl-9H-carbazole-3-carbaldehyde were added to 30 ml of EtOH, then the mixture was subjected to 4 h stirred and reflux conditions. The mixture was subjected to vacuum until its volume was reduced to 1.5 ml, adding of 40 ml dry of ether resulted in a product precipitation which was washed thoroughly with n-hexane.

Yield: 80% yellow powder with m. p = 185 °C. ^1H NMR (400 MHz, CDCl_3) δ (ppm): 1.3 (t, 3H, CH_3 of ethyl), 2.3 (s, 3H, CH_3 -Ph), 4.5 (q, 3H, CH_2 -CH₂), 7–8 (m, 10H, Ph), 8.3 (s, 1H, $>\text{C}=\text{N}-$), 11.5 (s, 1H, $-\text{NH}=\text{N}=\text{C}$).

2.3. Computation

All the DFT calculation were performed via Gaussian 09 software under DFT 6-311G(d,p) level theory.

3. Results and discussion

3.1. Preparation, CHN-EA and MS

In ethanol solvent, the condensation of 1:1 M ratio of 4-methyl benzenesulfonohydrazide with the aldehyde in an open atmosphere reflux condition formed the desired benzenesulfonohydrazide (ECMMBSH) in high yield (Scheme 1). The new ECMMBSH has a yellow color and solid in its nature, highly soluble

in CH_2Cl_2 , DMF, and DMSO, lower solubility in MeOH and water, and insoluble n-hexane.

The desired ECMMBSH was identified using CHN-EA, MS, FT-IR, NMR, TG/DTG and UV-Vis. Moreover, the DFT stimulation like optimization, MEP, LUMO/HOMO, DOS and TD-DFT under DFT 6-311G(d,p) level.

CHN-elemental analysis and MS of the ECMMBSH agreement well with it proposed molecular formula. For $\text{C}_{22}\text{H}_{21}\text{N}_3\text{O}_2\text{S}$, Calcd. C, 67.50; and H, 5.41%; found C, 67.30; and H, 5.3%. The TOF-MS of the ECMMBSH was in consistent with formula: $m/z = 391.1$ [M^+] (theo. $m/z = 391.5$). The atomic content and purity have been verified by EDX, the spectrum of EDX reflected the existence of O, N, C, and S only corresponding to the empirical formula of ECMMBSH ligand.

3.2. Optimized, MEP and MAC/NPA

The ECMMBSH ligand structure was subjected to DFT-B3LYP optimization as seen in Fig. 1a. The DFT gaseous state optimization revealed the ECMMBSH with E-isomer and not Z-one and this is not surprising since in gaseous state the e-isomers exhibits a lower internal repulsion energy compared to Z-isomer. Moreover, the calculated angles and bond length values for the ECMMBSH E-isomer are illustrated in Table 1. The MEP map calculation shows the surface of ECMMBSH with three colors: the high e-rich positions characterized by a red color that covered the O atoms of SO_2 groups and N of imine Schiff base functional group, the H of aromatic and ethyl function group has a blue color due to its e-poor aspects, deep blue color distinguished the H in HN reflecting it as e-poorer proton, the third functional groups were found to be neutral since they are green in color as seen in Fig. 1b. To evaluate the charge of each atom in ECMMBSH NPA and MAC calculation charge models were performed as seen in Fig. 1b and Table 2. Generally, NPA and MAC supported MEP calculation resulting in all the O and N atoms of Schiff base with negative in charge, meanwhile, the S and all protons atoms with positive charge, as expected, the proton of amine was detected with the highest positive charge as seen Fig. 1c and Table 2. Both NPA and MAC charge models coincided in measuring the charge of each atom of ECMMBSH since the degree of compatibility reached almost 90%, as seen in Fig. 1d

3.3. ^1H NMR of ECMMBSH

The exp. and theo. ^1H NMR spectra of the ECMMBSH were performed in CDCl_3 as in Fig. 2, Fig. 2a reflects the ^1H NMR spectra, the triplet signal for CH_3 of ethyl group was detected at $\delta \sim 1.3$ ppm, the single at $\delta \sim 2.3$ ppm attributed to Me of CH_3 -Ph part in ECMMBSH, the quartet signal for CH_2 of ethyl group was detected at $\delta \sim 4.5$ ppm, the Ph's protons were recorded in between 7 and 8 ppm, the (N=CH) azomethine proton signal was recorded at $\delta \sim 8.3$ ppm, signal for the proton of N-H was recorded at $\delta \sim 11.5$ ppm. The theoretical and experimental ^1H NMR of ECMMBSH ligand (Fig. 2b) reflected an excellent degree of matching with 0.9992 graphical correlation as seen in Fig. 2c. Moreover, only a slight shift in the chemical shifts for each proton were recorded by comparing individually the experimental to theoretical ^1H NMR. Unfortunately, due to lack in the solubility of ECMMBSH in deuterated solvents ^{13}C NMR was very weak to be reported.

3.4. IR

FT-IR was used to monitor the formation reactions of the desired ECMMBSH before and after mixing the starting materials. The individually FT-IR spectra of both 4-methyl-benzenesulfonohydrazide and the aldehyde were compared to the product ECMMBSH (after allowing it to condense) as see in Fig. 3a. The ECMMBSH formation

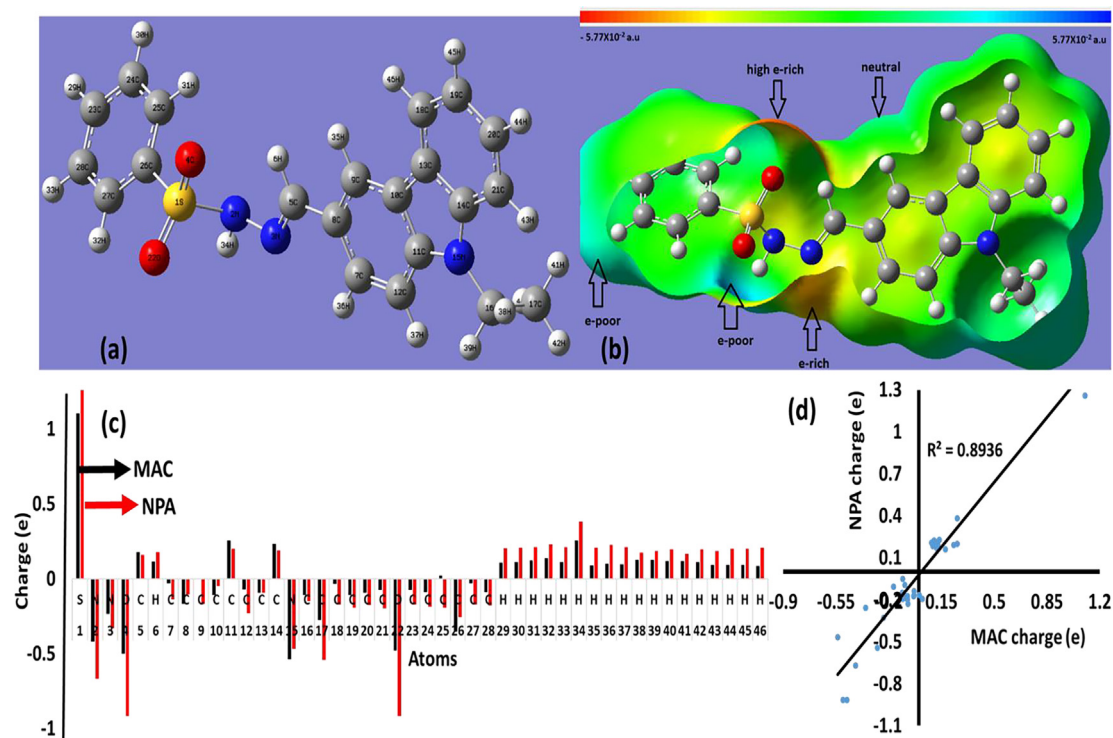
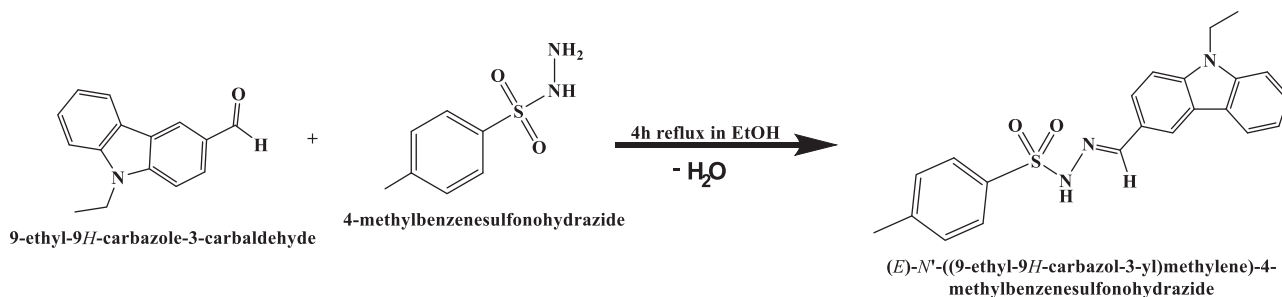


Fig. 1. (a) Optimized, (b) MEP, (c) MAC/NPA charge, and (d) MAC vs. NPA charge.

was supported *via* two major findings: (1). The stretching vibration N-H₂ in 4-methyl-benzenesulfonylhydrazide at 3383 cm⁻¹ was totally absent and the NH at 3254 cm⁻¹ displayed a down shift to 3152 cm⁻¹ as in Fig. 3a and (2) the C=O stretching of the aldehyde at 1679 cm⁻¹ was shifted to 1590 cm⁻¹ supporting the formation C=N- functional group as seen Fig. 3c.

The theoretical DFT-IR of ECMMBSH was performed to evaluate the degree of similarity to the experimental IR as shown in Fig. 3d. The exp. IR and the DFT theoretical wavenumbers resulted a linear relationship with 0.989 correlation coefficient reflecting excellent agreement as in Fig. 3e.

3.5. UV-Vis, HOMO/LUMO, DOS, and Tauc's optical gap

The UV-Visible of the ECMMBSH and its starting material were recorded in methanol as seen Fig. 4a. The UV-Vis measurements of the ECMMBSH showed a compensation of both the UV-Vis the aldehyde and 4-methyl-benzene-sulfonylhydrazide reactants. The UV-Vis of the ECMMBSH showed highly intense transitions bands with two heads at $\lambda_{\max} = 233$ and 241 nm with $\epsilon = 3.0 \times 10^4 \text{ M}^{-1} \text{ L}^{-1}$, intense band with $\lambda_{\max} = 297$ nm with $\epsilon = 5.0 \times 10^4 \text{ M}^{-1} \text{ L}^{-1}$,

and weak band at 323 nm with $\epsilon = 1.0 \times 10^4 \text{ M}^{-1} \text{ L}^{-1}$, these bands corresponded mostly to the $\pi-\pi^*$, $\pi-n$ and $n-\pi^*$ *e*-transfer respectively. The LUMO/HOMO shape and energy levels were schematic performance in methanol solvent as seen in Fig. 4b. In the HOMO electrons distribution over the orbitals focused on aldehyde part of ECMMBSH with -5.597385 eV, meanwhile, the LUMO focused on the 4-methylbenzenesulfonylhydrazide with part of ECMMBSH with -1.527 eV, the energy gap found to be $\Delta E_{\text{HOMO/LUMO}} = 4.071$ eV as illustrated in Fig. 4b. The DOS energy gap calculated was $\Delta E_{\text{DOS}} = 4.161$ eV as seen in Fig. 4c; the two ΔE of both LUMO/HOMO and DOS values showed a rather high convergence as seen in Fig. 4c. The experiment optical energy gap value of ECMMBSH in methanol solvent using the Tauc's equation was evaluated as in Fig. 4d. The optical energy gap found to be $= 3.987$ eV, such seen is highly proportionate with the $\Delta E_{\text{HOMO/LUMO}}$ and ΔE_{DOS} DFT-calculated values.

3.6. TD-DFT/UV-Vis. and TG/DTG

The UV-Visible behaviors of the ECMMBSH in MeOH in both experimental and theoretical TD-DFT in the 200–800 nm range

Table 1
Angles and bond distances of DFT-optimized ECMMBSH structure.

No.	Bond		Å	No.	Angle			(°)
1	S1	N2	1.7471	1	N2	S1	O4	106.34
2	S1	O4	1.4589	2	N2	S1	O22	111.64
3	S1	O22	1.4617	3	N2	S1	C26	98.54
4	S1	C26	1.7981	4	O4	S1	O22	120.31
5	N2	N3	1.4159	5	O4	S1	C26	109.9
6	N3	C5	1.2834	6	O22	S1	C26	107.94
7	C5	C8	1.4607	7	S1	N2	N3	118.61
8	C7	C8	1.4144	8	N2	N3	C5	116.45
9	C7	C12	1.3829	9	N3	C5	C8	121.24
10	C8	C9	1.3985	10	C8	C7	C12	121.62
11	C9	C10	1.3931	11	C5	C8	C7	121.65
12	C10	C11	1.4192	12	C5	C8	C9	118.7
13	C10	C13	1.4471	13	C7	C8	C9	119.65
14	C11	C12	1.401	14	C8	C9	C10	119.8
15	C11	N15	1.3839	15	C9	C10	C11	119.48
16	C13	C14	1.4183	16	C9	C10	C13	133.93
17	C13	C18	1.3969	17	C11	C10	C13	106.59
18	C14	N15	1.3925	18	C10	C11	C12	121.24
19	C14	C21	1.396	19	C10	C11	N15	109.2
20	N15	C16	1.4558	20	C12	C11	N15	129.56
21	C16	C17	1.5317	21	C7	C12	C11	118.2
22	C18	C19	1.3897	22	C10	C13	C14	106.51
23	C19	C20	1.4028	23	C10	C13	C18	133.95
24	C20	C21	1.3911	24	C14	C13	C18	119.54
25	C23	C24	1.3958	25	C13	C14	N15	109.04
26	C23	C28	1.3929	26	C13	C14	C21	121.48
27	C24	C25	1.3903	27	N15	C14	C21	129.49
28	C25	C26	1.394	28	C11	N15	C14	108.65
29	C26	C27	1.392	29	C11	N15	C16	125.71
30	C27	C28	1.3938	30	C14	N15	C16	125.58

Table 2
MAC/NPA charge of each atom in ECMMBSH.

No.	Atom	MAC	NPA	No.	Atom	MAC	NPA
1	S	1.102349	1.25898	24	C	-0.09003	-0.18476
2	N	-0.41945	-0.66874	25	C	0.022174	-0.19506
3	N	-0.23341	-0.32983	26	C	-0.35388	-0.25651
4	O	-0.50273	-0.91461	27	C	-0.03119	-0.16986
5	C	0.176066	0.1594	28	C	-0.08816	-0.18026
6	H	0.114058	0.17843	29	H	0.108079	0.20442
7	C	-0.03211	-0.13894	30	H	0.108734	0.20669
8	C	-0.167	-0.10554	31	H	0.121761	0.21069
9	C	0.001131	-0.16625	32	H	0.136436	0.22777
10	C	-0.10824	-0.04908	33	H	0.109181	0.20926
11	C	0.253734	0.19796	34	H	0.253581	0.38121
12	C	-0.0715	-0.23038	35	H	0.086581	0.20861
13	C	-0.09429	-0.09352	36	H	0.099677	0.22447
14	C	0.231138	0.1893	37	H	0.096323	0.2097
15	N	-0.53929	-0.46854	38	H	0.126264	0.17164
16	C	-0.10897	-0.14935	39	H	-0.126877	0.18623
17	C	-0.27571	-0.54127	40	H	0.118902	0.19529
18	C	-0.03525	-0.17226	41	H	0.118822	0.16533
19	C	-0.10802	-0.19485	42	H	0.110407	0.19752
20	C	-0.09466	-0.17437	43	H	0.093428	0.18332
21	C	-0.07636	-0.19811	44	H	0.091595	0.20057
22	O	-0.47771	-0.91662	45	H	0.091185	0.1991
23	C	-0.0748	-0.17287	46	H	0.084282	0.20566

are shown seen Fig. 5a. In general, the three experimental main peaks at $\lambda_{\max} = 233, 297, 323$ nm that sited to $\pi-\pi^*$, $\pi-n$ and $n-\pi^*$, e -transitions respectively in Fig. 5a was supported theoretically via TD-DFT computation. The TD-DFT of the ECMMBSH showed again a three-band in the UV area with $\lambda_{\max} = 224$ nm attributed mainly to HOMO→LUMO (92%), meanwhile the visible band $\lambda_{\max} = 278$ nm attributed mainly to H-1→L + 1 (85%), and $\lambda_{\max} = 335$ nm attributed to H-4→L + 2 (69%) (Fig. 5b). The detail of TD-DFT information like wavelength (nm), calculated energy (cm^{-1}) and transition oscillator strength (f) of the first 16 bands (with $f > 0.01$) are illustrated in Table 3. Moreover, several solvents,

such as CH_2Cl_2 , DMSO and DMF, have been tried; however, they do not alter the electronic behaviors of ECMMBSH, either in theory or in experimental fields. In conclusion, theoretical TD-DFT and the experimental UV-visible behavior of ECMMBSH are in an acceptable correlation.

The TG/DTG attitude of ECMMBSH ligand was achieved in 22–900 °C temperature scale with 10 °Cmin⁻¹ heating rate at open room temperature condition (Fig. 5b). The ECMMBSH ligand was found to be stable up to ~160 °C without any loss in its mass, at temperature higher than 160 °C the molecule started to decompose via two broad steps, the first step was outset from 160 °C

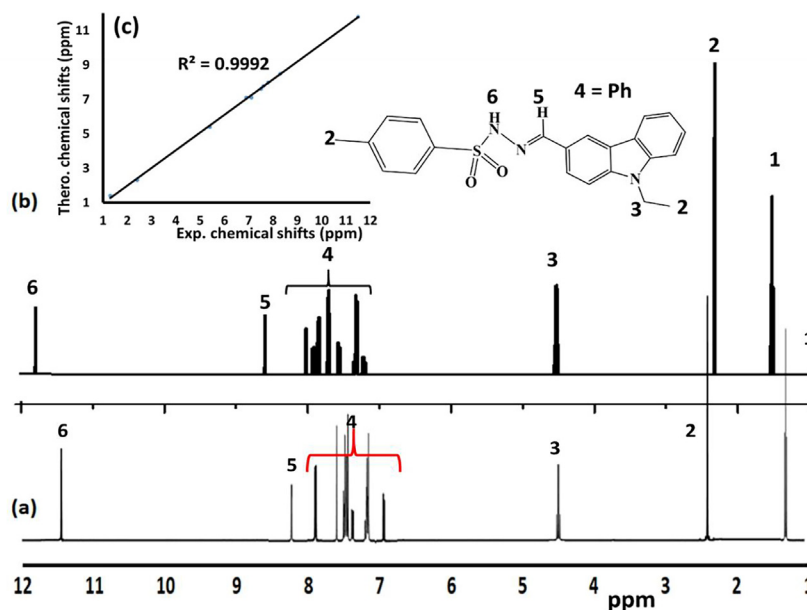


Fig. 2. ^1H NMR spectra of ECMMBSH in CDCl_3 (a) Experimental, (b) Theoretical, and (c) Experimental vs. theoretical chemical shifts relation.

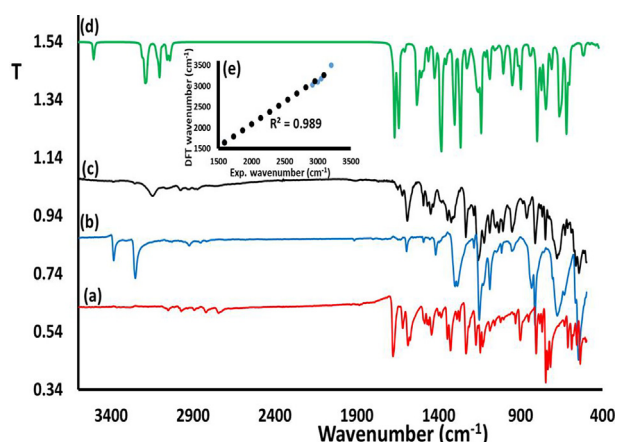


Fig. 3. Exp. FT-IR spectra recorded for (a) the aldehyde b) 4-methyl-benzene-sulfonylhydrazide, c) ECMMBSH (d) DFT-IR of ECMMBSH, and (e) DFT/Exp.-IR relation.

and finished at $320\text{ }^\circ\text{C}$ with $T_{\text{DTA}} = 282\text{ }^\circ\text{C}$ and $\sim 38\%$ mass lost. The 2nd step was outset from $480\text{ }^\circ\text{C}$ and end at $610\text{ }^\circ\text{C}$ with $T_{\text{DTA}} = 520\text{ }^\circ\text{C}$ and $\sim 62\%$ mass lost. Moreover, the pure organic ECMMBSH ligand was usually decomposed completely to light gasses (CO , CO_2 , NO_x and SO_x) since at the end of the decomposition process zero mass residue was observed as seen in Fig. 5b.

3.7. A naked eye and spectroscopy colorimetric Cu^{2+} sensor

The colorimetric naked eye behavior of the ECMMBSH (light yellow) complexation with CuX_2/MeOH (for example $\text{CuBr}_2/\text{MeOH}$, brown) before and after direct mixed to produced $\text{CuX}_2\text{-(ECMMBSH)}_2$ ($\text{X} = \text{NO}_3$ complex 1, Cl complex 2 and Br complex 3) (has been illustrated in Fig. 6. The absorption of ECMMBSH in the presence of CuX_2/MeOH was displayed in Fig. 6a. Due to the complexation between the ECMMBSH and Cu(II) solution the color was changed to green without depending on the X ligand, a slight shift in maximum was observed, $\text{Cu(NO}_3)_2/\text{ECMMBSH}$ revealed with $\lambda_{\text{max}} = 611\text{ nm}$, $\text{CuCl}_2/\text{ECMMBSH}$ revealed with $\lambda_{\text{max}} = 626\text{ nm}$ and $\text{CuBr}_2/\text{ECMMBSH}$ revealed with $\lambda_{\text{max}} = 633\text{ nm}$ in Fig. 6a. The

shifts in λ_{max} values are consistent with d-splitting field theory and spectrophotometric series strength since $\text{NO}_3 > \text{Cl} > \text{Br}$ ligands strength are recorded as Fig. 6a. The ECMMBSH displayed a remarkable sensitivity to Cu(II) solution even at very low copper concentration. The visible complexation process of $\text{CuBr}_2/\text{MeOH}$ with ECMMBSH/MeOH was monitored in between 500 and 1000 nm. The peak at 890 nm that characteristic of $1 \times 10^{-3}\text{ M}$ pure brown $\text{CuBr}_2/\text{MeOH}$ solution absorbance gradually and rapidly decreased by the addition of excess ECMMBSH/MeOH ($1 \times 10^{-2}\text{ M}$) parallel to the appearance of the green $\text{CuBr}_2(\text{ECMMBSH})_2$ complex at $\lambda_{\text{max}} = 633\text{ nm}$ with one isosbestic point at $\lambda_{\text{max}} 770\text{ nm}$. The colorimetric complexation of ECMMBSH with $\text{CuBr}_2/\text{MeOH}$ at RT was found to be very fast, as one minute was sufficient to complete this process considering that a measurement every $\sim 10\text{ s}$ was recorded as displayed in Fig. 6b.

4. Conclusion

Benzene-sulfonylhydrazide (ECMMBSH) ligand was made available in a very high yield. The condensation reaction was successfully monitored via UV-Vis and IR spectroscopy. Moreover, the product was characterized via CHN-EA, MS, ^1H NMR, EDX, CHN-EA, UV-Vis., IR, and TGA thermal analysis. The ECMMBSH ligand showed a high stability, in addition, it decomposed in two steps. The DFT-optimized, MEP and MAC/NPA were performed for ECMMBSH, the HOMO/LUMO and DOS calculated energy levels supported the Tuac experimental optical energy gap result. The TD-DFT and UV-vis. experimental absorption behaviors in MeOH solvent were in high agreement degree, moreover, the ECMMBSH colorimetric sensation effect towards Cu^{2+} ions was figure out via the naked eye and UV-spectrophotometric method. The time-dependent chemo-sensation complexation of $\text{CuBr}_2/\text{MeOH}$ with ECMMBSH ligand was successfully monitored by UV-vis. Spectroscopy.

Declaration of Competing Interest

The authors declare that they have no known competing financial interests or personal relationships that could have appeared to influence the work reported in this paper.

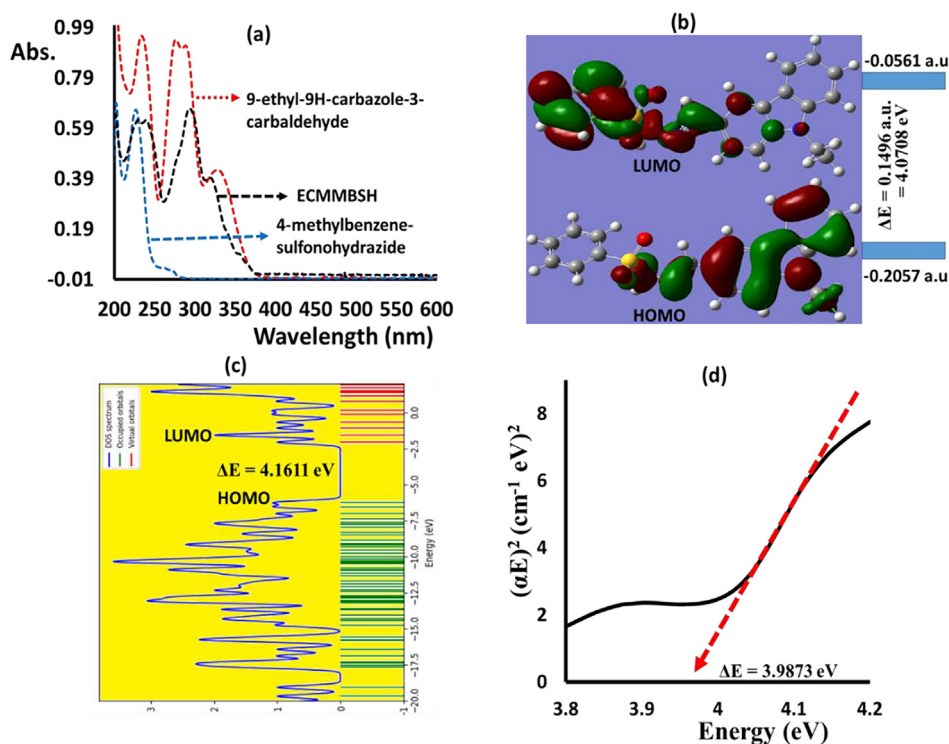


Fig. 4. (a) RT Experimental UV-Vis. spectra, (b) HOMO/LUMO energy diagrams, (c) DOS, and (d) Exp. Tauc's energy gap of the ECMMBSH in methanol.

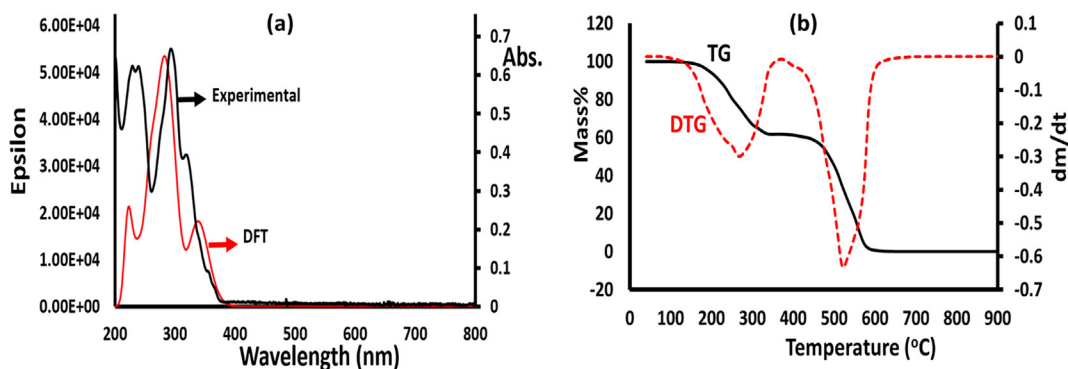


Fig. 5. (a) TD-DFT/UV-vis. spectra, and (b) TG/DTG of ECMMBSH.

Table 3

TD-DFT computation of ECMMBSH in methanol.

No.	E (cm ⁻¹)	λ (nm)	Osc. Str. (f)	Major contribution
1	29083.5	343.8	0.1608	HOMO→LUMO (92%)
2	30298.2	330.0	0.1179	H-2→LUMO (39%), H-1→LUMO (49%)
3	32471.0	307.9	0.0044	H-2→LUMO (23%), H-1→LUMO (14%), HOMO→L + 1 (54%)
4	33998.6	294.1	0.4111	H-2→LUMO (24%), H-1→LUMO (33%), HOMO→L + 1 (31%)
5	35917.4	278.4	0.5194	H-1→L + 1 (85%)
6	38240.3	261.5	0.3456	H-3→LUMO (84%)
7	39133.2	255.53	0.0488	H-2→L + 1 (45%), HOMO→L + 4 (38%)
8	40076.0	249.5	0.0186	H-4→LUMO (86%)
9	40093.0	249.4	0.0833	H-3→L + 1 (10%), H-2→L + 1 (42%), HOMO→L + 4 (30%)
10	41622.2	240.2	0.0608	H-3→L + 1 (46%), H-1→L + 4 (30%), HOMO→L + 4 (15%)
11	41990.8	238.1	0.0102	H-5→L + 2 (50%), H-4→L + 3 (31%)
12	42484.4	235.3	0.0728	H-6→LUMO (55%), H-1→L + 4 (25%)
13	44204.0	226.2	0.0005	H-2→L + 3 (82%), H-1→L + 3 (10%)
14	44332.2	225.5	0.0305	H-8→LUMO (12%), H-7→LUMO (24%), H-3→L + 2 (50%)
15	45066.2	221.9	0.0879	H-3→L + 1 (14%), H-1→L + 4 (18%), H-1→L + 5 (10%), HOMO→L + 5 (31%)
16	45370.3	220.4	0.1498	H-4→L + 2 (69%)

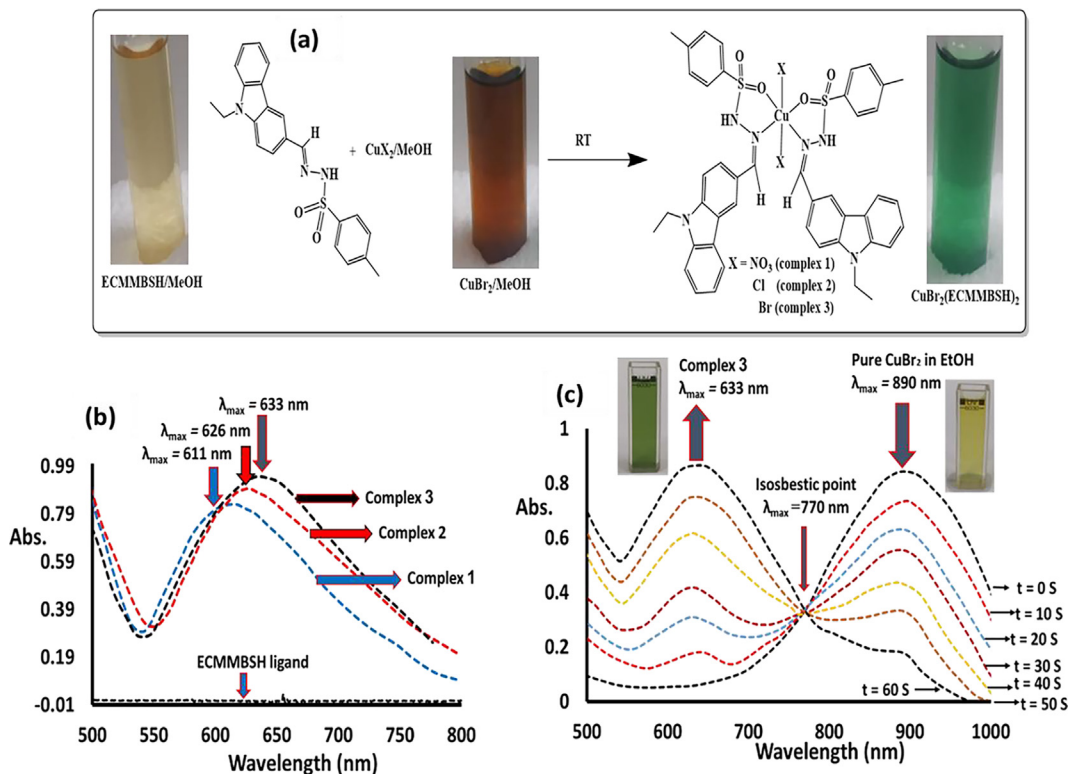


Fig. 6. (a) Necked eye colorimetric complexation of ECMMBSH with CuX_2/MeOH , (b) Absorption behavior of ECMMBSH with CuX_2/MeOH ($\text{X} = \text{NO}_3$ complex 1, Cl complex 2 and Br complex 3), and (c) Time-dependence of complexation of $\text{CuBr}_2/\text{MeOH}$ with ECMMBSH ligand.

Acknowledgement

The authors extend their appreciation to the Researchers Supporting Project number (RSP-2021/381), King Saud University, Riyadh, Saudi Arabia.

References

- Abbasi, Z., Salehi, M., Khaleghian, A., Kubicki, M., 2018. In vitro cytotoxic activity of a novel Schiff base ligand derived from 2-hydroxy-1-naphthaldehyde and its mononuclear metal complexes. *J. Mol. Struct.* 1173, 213–220.
- Ahmadi, R.A., Amani, S., 2012. Synthesis, spectroscopy, thermal analysis, magnetic properties and biological activity studies of Cu (II) and Co (II) complexes with Schiff base dye ligands. *Molecules* 17 (6), 6434–6448.
- Al-Rimawi, F., Rishmawi, S., Ariqat, S.H., Khalid, M.F., Warad, I., Salah, Z., 2016. Anticancer activity, antioxidant activity, and phenolic and flavonoids content of wild *Tragopogon porrifolius* plant extracts. *Evidence-Based Complement. Altern. Med.*, 2016.
- Al-Zaqri, N., Khatib, T., Alsalmeh, A., Alharthi, F.A., Zarrouk, A., Warad, I., 2020a. Synthesis and amide imidic prototropic tautomerization in thiophene-2-carbohydrazide: XRD, DFT/HSA-computation, DNA-docking, TG and isothermal kinetics via FWO and KAS models. *RSC Adv.* 10 (4), 2037–2048.
- Al-Zaqri, N., Salih, K.S.M., Awwadi, F.F., Alsalmeh, A., Alharthi, F.A., Alsyahi, A., Ali, A. A., Zarrouk, A., Aljohani, M., Chetouni, A., Warad, I., 2020b. Synthesis, physicochemical, thermal, and XRD/HSA interactions of mixed $[\text{Cu}(\text{Bipy})(\text{Dipn})\text{X}]_2$ complexes: DNA binding and molecular docking evaluation. *J. Coord. Chem.* 73 (23), 3236–3248.
- Badran, I., Abdallah, L., Mubarakheh, R., Warad, I., 2019. Effect of alkyl derivation on the chemical and antibacterial properties of newly synthesized Cu(II)-diamine complexes. *Moroccan J. Chem.* 7, 1–7.
- Badran, I., Tighadouini, S., Radi, S., Zarrouk, A., Warad, I., 2021. Experimental and first-principles study of a new hydrazine derivative for DSSC applications. *J. Mol. Struct.* 1229, 129799. <https://doi.org/10.1016/j.molstruc.2020.129799>.
- Chatterjee, A.K., Chakraborty, R., Basu, T., 2014. Mechanism of antibacterial activity of copper nanoparticles. *Nanotechnology* 25 (13), 135101.
- Das, D.K., Deka, S., Guha, A.K., 2019. Schiff Base Derived from 4, 4'-methylene dianiline and p-anisaldehyde: colorimetric Sensor for Cu^{2+} , Paper Strip Sensor for Al^{3+} and Fluorescent Sensor for Pb^{2+} . *J. Fluoresc.* 29 (6), 1467–1474.
- Dehghani-Firouzabadi, A.A., Motevaseliyan, F., 2014. Synthesis and characterization of four new unsymmetrical potentially pentadentate Schiff base ligands and related Zn(II) and Cd(II) complexes. *Eur. J. Chem.* 5 (4), 635–638.
- Despaigne, A.A.R., Silva, J.G.d., Carmo, A.C.M.d., Sives, F., Piro, O.E., Castellano, E.E., Beraldo, H., 2009. Copper (II) and zinc (II) complexes with 2-formylpyridine-derived hydrazones. *Polyhedron* 28 (17), 3797–3803.
- Eckenhoff, W.T., Biernesser, A.B., Pintauer, T., 2012. Structural characterization and investigation of iron (III) complexes with nitrogen and phosphorus based ligands in atom transfer radical addition (ATRA). *Inorg. Chim. Acta* 382, 84–95.
- Hossain, M.E., Alam, M.N., Begum, J., Akbar Ali, M., Nazimuddin, M., Smith, F.E., Hynes, R.C., 1996. The preparation, characterization, crystal structure and biological activities of some copper(II) complexes of the 2-benzoylpyridine Schiff bases of S-methyl- and S-benzylthiocarbamate. *Inorg. Chim. Acta* 249 (2), 207–213.
- Hu, S., Song, J., Zhao, F., Meng, X., Wu, G., 2015. Highly sensitive and selective colorimetric naked-eye detection of Cu^{2+} in aqueous medium using a hydrazine chemosensor. *Sens. Actuators B Chem.* 215, 241–248.
- Jang, H.J., Jo, T.G., Kim, C., 2017. A single colorimetric sensor for multiple targets: the sequential detection of Co^{2+} and cyanide and the selective detection of Cu^{2+} in aqueous solution. *RSC Adv.* 7 (29), 17650–17659.
- Johnson, J., Dhanaraj, C.J., 2020. Biological and molecular modeling studies on some transition metal (II) complexes of a quinoxaline based ONO donor bishydrazone ligand. *J. Biomol. Struct. Dyn.*, 1–13.
- Khan, K.M., Taha, M., Naz, F., Ali, S., Perveen, S., Choudhary, M.I., 2012. Synthesis of acylhydrazide Schiff bases and their anti-oxidant activity. *Med. Chem* 8, 705–710.
- Konstantinovic, S., Radovanovic, B., Kacic, Z., Vasic, V., 2003. Synthesis and characterization of Co (II), Ni (II), Cu (II) and Zn (II) complexes with 3-salicylidenehydrazono-2-indolinone. *J. Serbian Chem. Soc.* 68 (8-9), 641–647.
- Lindner, E., Warad, I., Eichele, K., Mayer, H.A., 2003. Supported organometallic complexes Part 34: synthesis and structures of an array of diamine (ether-phosphine) ruthenium (II) complexes and their application in the catalytic hydrogenation of trans-4-phenyl-3-butene-2-one. *Inorg. Chim. Acta* 350, 49–56.
- Lu, Z., Eichele, K., Warad, I., Mayer, H.A., Lindner, E., Jiang, Z., Schurig, V., 2003. Supported Organometallic Complexes. XXXVIII [1] Bis (methoxyethylidimethylphosphine) ruthenium (II) Complexes as Transfer Hydrogenation Catalysts. *Zeitschrift für Anorg. und Allg. Chemie* 629, 1308–1315.
- Masoud, M.S., Ibrahim, A.A., Khalil, E.A., El-Marghany, A., 2007. Spectral properties of some metal complexes derived from uracil-thiouacil and citrazinic acid compounds. *Spectrochim. Acta Part A Mol. Biomol. Spectrosc.* 67 (3-4), 662–668.

- Maurya, M.R., Dhaka, S., AVECILLA, F., 2015. Oxidative bromination of monoterpene (thymol) using dioxidomolybdenum (VI) complexes of hydrazones of 8-formyl-7-hydroxy-4-methylcoumarin. *Polyhedron* 96, 79–87.
- Pervaiz, M., Ahmad, I., Yousaf, M., Kirn, S., Munawar, A., Saeed, Z., Adnan, A., Gulzar, T., Kamal, T., Ahmad, A., Rashid, A., 2019. Synthesis, spectral and antimicrobial studies of amino acid derivative Schiff base metal (Co, Mn, Cu, and Cd) complexes. *Spectrochim. Acta Part A Mol. Biomol. Spectrosc.* 206, 642–649.
- Rajasekar, M., Sreedaran, S., Prabu, R., Narayanan, V., Jegadeesh, R., Raaman, N., Kalilur Rahiman, A., 2010. Synthesis, characterization, and antimicrobial activities of nickel (II) and copper (II) Schiff-base complexes. *J. Coord. Chem.* 63 (1), 136–146.
- Rbaa, M., Abousalem, A.S., Touhami, M.E., Warad, I., Bentiss, F., Lakhri, B., Zarrouk, A., 2019. Novel Cu (II) and Zn (II) complexes of 8-hydroxyquinoline derivatives as effective corrosion inhibitors for mild steel in 1.0 M HCl solution: computer modeling supported experimental studies. *J. Mol. Liq.* 290, 111243.
- Rouifi, Z., Benhiba, F., Faydy, M.E., Laabaissi, T., About, H., Oudda, H., Warad, I., Guenbour, A., Lakhri, B., Zarrouk, A., 2019. Performance and computational studies of new soluble triazole as corrosion inhibitor for carbon steel in HCl. *Chem. Data Collect.* 22, 100242. <https://doi.org/10.1016/j.cdc.2019.100242>.
- Routier, S., Bernier, J.-L., Waring, M.J., Colson, P., Houssier, C., Bailly, C., 1996. Synthesis of a functionalized Salen–Copper complex and its interaction with DNA. *J. Org. Chem.* 61 (7), 2326–2331.
- Saleemh, F.A., Musameh, S., Sawafta, A., Brandao, P., Tavares, C.J., Ferdov, S., Barakat, A., Ali, A.A., Al-Noaimi, M., Warad, I., 2017. Diethylenetriamine/diamines/copper (II) complexes [Cu (dien)(NN)] Br 2: synthesis, solvatochromism, thermal, electrochemistry, single crystal, Hirshfeld surface analysis and antibacterial activity. *Arab. J. Chem.* 10 (6), 845–854.
- Shafaatian, B., Mousavi, S.S., Afshari, S., 2016. Synthesis, characterization, spectroscopic and theoretical studies of new zinc (II), copper (II) and nickel (II) complexes based on imine ligand containing 2-aminothiophenol moiety. *J. Mol. Struct.* 1123, 191–198.
- Sousa, I., Claro, V., Pereira, J.L., Amaral, A.L., Cunha-Silva, L., de Castro, B., Feio, M.J., Pereira, E., Gameiro, P., 2012. Synthesis, characterization and antibacterial studies of a copper (II) levofloxacin ternary complex. *J. Inorg. Biochem.* 110, 64–71.
- Trzesowska-Kruszynska, A., 2012. Copper complex of glycine Schiff base: In situ ligand synthesis, structure, spectral, and thermal properties. *J. Mol. Struct.* 1017, 72–78.
- Warad, I., Al-Demeri, Y., Al-Nuri, M., Shahwan, S., Abdoh, M., Naveen, S., Lokanath, N.K., Mubarak, M.S., Ben Hadda, T., Mabkhot, Y.N., 2017a. Crystal structure, Hirshfeld surface, physicochemical, thermal and DFT studies of (N1E, N2E)-N1, N2-bis ((5-bromothiophen-2-yl) methylene) ethane-1, 2-diamine N2S2 ligand and its [CuBr(N2S2)]Br complex. *J. Mol. Struct.* 1142, 217–225.
- Warad, I., Awwadi, F.F., Daqqa, M., Al Ali, A., Ababneh, T.S., AlShboul, T.M.A., Jazazi, T.M.A., Al-Rimawi, F., Hadda, T.B., Mabkhot, Y.N., 2017b. New isomeric Cu(NO₂-phen)2Br complexes: Crystal structure, Hirshfeld surface, physicochemical, solvatochromism, thermal, computational and DNA-binding analysis. *J. Photochem. Photobiol. B Biol.* 171, 9–19.
- Warad, I., Khan, A.A., Azam, M., Al-Resayes, S.I., Haddad, S.F., 2014. Design and structural studies of diimine/CdX₂ (X= Cl, I) complexes based on 2, 2-dimethyl-1, 3-diaminopropane ligand. *J. Mol. Struct.* 1062, 167–173.
- Warad, I., Musameh, S., Badran, I., Nassar, N.N., Brandao, P., Tavares, C.J., Barakat, A., 2017c. Synthesis, solvatochromism and crystal structure of *trans*-[Cu (Et₂NCH₂CH₂NH₂)₂.H₂O](NO₃)₂ complex: experimental with DFT combination. *J. Mol. Struct.* 1148, 328–338.
- Warad, I., Suboh, H., Al-Zaqri, N., Alsalmeh, A., Alharthi, F.A., Aljohani, M.M., Zarrouk, A., 2020. Synthesis and physicochemical, DFT, thermal and DNA-binding analysis of a new pentadentate N 3 S 2 Schiff base ligand and its [CuN₃S₂]²⁺ complexes. *RSC Adv.* 10 (37), 21806–21821.
- Wu, L.-M., Teng, H.-B., Ke, X.-B., Xu, W.-J., Su, J.-T., Liang, S.-C., Hu, X.-M., 2007. Copper(II) complexes of salicylaldehyde hydrazones: synthesis, structure, and DNA interaction. *Chem. Biodivers.* 4 (9), 2198–2209.